JOURNAL OF GEOPHYSICAL RESEARCH, VOL. 95, NO. B2, PAGES 1223–1237, FEBRUARY 10, 1990

# Heat Flow Through the Sea Bottom Around the Yucatan Peninsula

M. D. KHUTORSKOY,[1] R. FERNANDEZ,[2] V. I. KONONOV,[1] B. G. POLYAK,[1]
V. G. MATVEEV,[3] AND A. A. ROT[3]

Heat flow studies were conducted in January–February 1987, off the Atlantic Coast of Mexico on board the R/V *Akademik Nikolai Strakhov*. Two areas were surveyed, one transecting the Salt Dome Province and the Campeche Canyon, in the Gulf of Mexico, and the other, on the eastern flank of the Yucatan Peninsula. Conductive heat flow through the bottom sediments was determined as the product of vertical temperature gradient and in situ thermal conductivity, measured with a thermal probe using a multithermistor array and real-time processing capabilities. Forward two-dimensional modeling allows us to estimate heat flow variations at both sites from local disturbances and to obtain average heat flow values of 51 mW/m$^2$ for the transect within the Gulf of Mexico and 38 and 69 mW/m$^2$ for two basins within the Yucatan area. Sea bottom relief has a predominant effect over other environmental factors in the scatter of heat flow determination in the Gulf of Mexico.

## INTRODUCTION

During the fourth expedition of the R/V *Akademik Nikolai Strakhov*, owned by the Geological Institute of the USSR Academy of Sciences, we conducted a detailed study on the geothermal conditions in the Gulf of Mexico and in the Caribbean Sea, within the exclusive economic zone of Mexico. This research was part of an ongoing joint scientific and technical cooperative project between Mexico and the USSR. Mexican and Soviet scientists took part in data collection and processing aboard the ship.

The principal objective of our study was aimed at gaining a better understanding of differing geothermal conditions on several oceanic bottom structures and also to examine the influence of halokinesis upon heat flow in oceanic bottom sediments.

Terrestrial heat flow measurements are necessary to understand the energy balance in geological processes, the overall geodynamic environments, and the geothermal resources. If a large scatter of heat flow data is obtained in the uppermost crustal horizons, it can prevent a clear identification of the regional background. To define the latter, detailed investigations are of uppermost importance, as exemplified by the recent work in the Bermuda Bank [*Detrick et al.*, 1986] and in the Cape Verde Islands [*Courtney and White*, 1986].

We have followed a similar approach in this study, in which gathering substantial amounts of data and simple two-dimensional forward modeling have allowed us to discern the effects of local disturbances upon heat flow in deep ocean basins. The background heat flow can reasonably be estimated once these disturbing influences are accounted for.

[1]Geological Institute of the Academy of Sciences of the USSR, Moscow.
[2]Department of Applied Geophysics, Centro de Investigacion Cientifica y Educación Superior de Ensenada, Ensenada, Baja California, Mexico.
[3]Polytechnical Institute, Kuybyshev, USSR.



Paper number 89JB01501.
0148-0227/90/89JB-01501$05.00

## GEOLOGICAL SETTINGS

We focused our efforts on two survey areas whose geographic and tectonic setting are shown in Figure 1. The first, located in the Gulf of Mexico, will be referred to as the Campeche transect and the other, situated in the Caribbean Sea, will be referred to as the Yucatan transect.

### *Campeche Transect*

This study area is situated on the southern part of the Gulf of Mexico in an east-northeast extension, transecting the Campeche Bank, the submeridional submarine canyon of the same name and the salt dome region to the west. All of these features are associated with the Coastal structural tectonic zone within the Gulf of Mexico depression [*Khain*, 1981] pertaining to the peripheral parts of the continent.

*Antoine and Pyle* [1970] report a layer of terrigeneous carbonate Meso-Cenozoic sediments up to 6 km thick, resting upon Paleozoic sediments, within this area. The lower section includes red beds overlain by evaporites, producing numerous salt diapirs. The evaporites are Triassic–Late Jurassic in age, but intensive halokinesis took place in the middle Miocene, about 9–12 m.y. ago [*Bertagne*, 1984]. The overlying sequence is pierced by relatively narrow salt diapirs (0.8–3.5 km in diameter), although they may have larger diameters in some areas (5–6 km). At some depth below the seafloor these salt diapirs merge, forming large masses and ridges. These are overlain by a caprock (limestone, anhydrites, gypsum, and clays) several tens to hundreds of meters thick. This trend continues into subareal parts of the Coastal zone on the southwest margin of the gulf where predominantly linear and brachi-anticlinal salt or gypsum-anhydrite plugs are found. The crustal thickness beneath the Campeche Bank is 30 km on the average, thinning to 20 km under the salt dome region [*Antoine and Pyle*, 1970].

### *Yucatan Transect*

The Yucatan transect is situated on the western flank of the Yucatan basin on the Caribbean Sea. The western part of this transect is located on the continental crust of the Yucatan platform. The Yucatan basin has an oceanic crust. Water depths near 4 km are common here. The Moho discontinuity (with $P$ wave velocities ($V_p$) near 8.1 km/s) is placed at 13 km below the seafloor overlaid by 6 km of

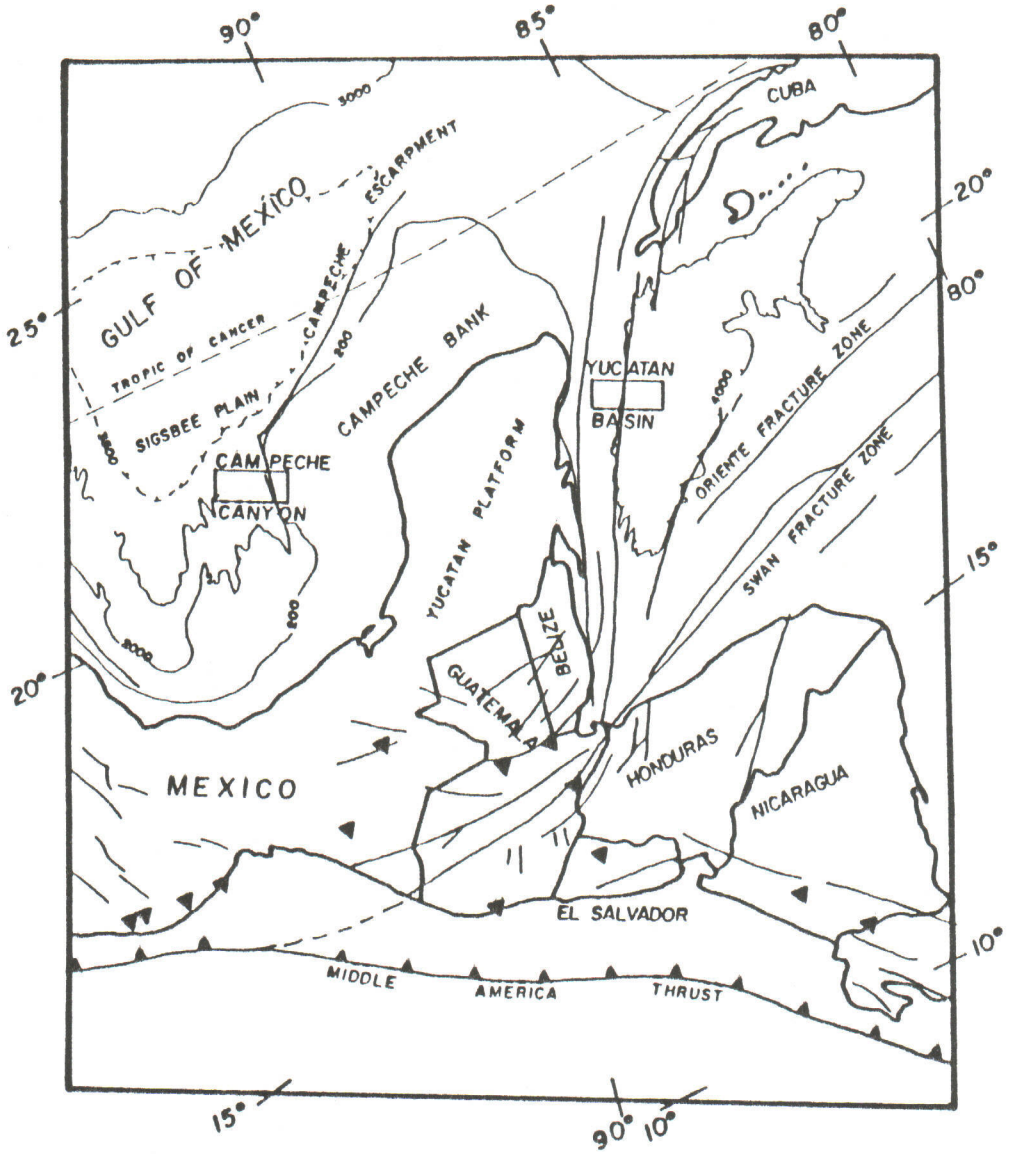


Fig. 1. Tectonic sketch of the studied areas modified from *Drummond* [1981] and *Case and Holcombe* [1980]. Triangles show epicenters of earthquakes with magnitudes greater than 7.5. The two studied areas are shown in small rectangles.

oceanic basalts ($V_p$ = 6.6–6.8 km/s) and approximately 3 km of sedimentary cover [*Edgar et al.*, 1971]. According to paleomagnetic data, the development of the Yucatan basin began as early as the Turonian [*Wadge et al.*, 1982].

The much more studied subareal Yucatan peninsula shows Neogene limestones on top of a Paleozoic continental block. A very pronounced submeridional fault, with an eastern downdrop, stretches along the eastern coastal margin of Yucatan peninsula. A subparallel major tectonic fault runs eastward from there and bends farther north bordering the coastline of Cuba and Haiti. Our study area transects this second lineament and also encompasses a narrow N-NW trending uplift (water depth near 300 m). This pronounced uplift is of tectonic origin, as evidenced by seismic work and divides the continental slope of the Yucatan peninsula into two basins, an "upper" basin (so-called East Yucatan basin) with water depths of 1.2 km and a "lower" basin, which is considerably deeper (4.5 km).

Samples of metamorphic rocks (muscovite and sericite schists) similar to those found in Juventud Island and in the Paleozoic strata of South Yucatan Peninsula were found on the slope leading to the lower basin by earlier dredging by *Dillon* [1972] and by that performed during the same leg of the R/V *Akademik Nikolai Strakhov*. Therefore it is believed that most of the continental crustal complex is made up of these rocks [*Pushcharovsky*, 1979; *Mossakovsky et al.*, 1986]. It seems that within the Yucatan transect there is a crustal suture zone, with Paleozoic continental crust being in contact with older oceanic Mesozoic material.

## Measurement Technique

Heat flow data were obtained using a digital geothermal probe system developed by *Matveev and Rot* [1988]. This probe (similar to a "violin-bow" design [*Hyndman et al.*, 1979]) measures the in situ temperature and thermal conduc-

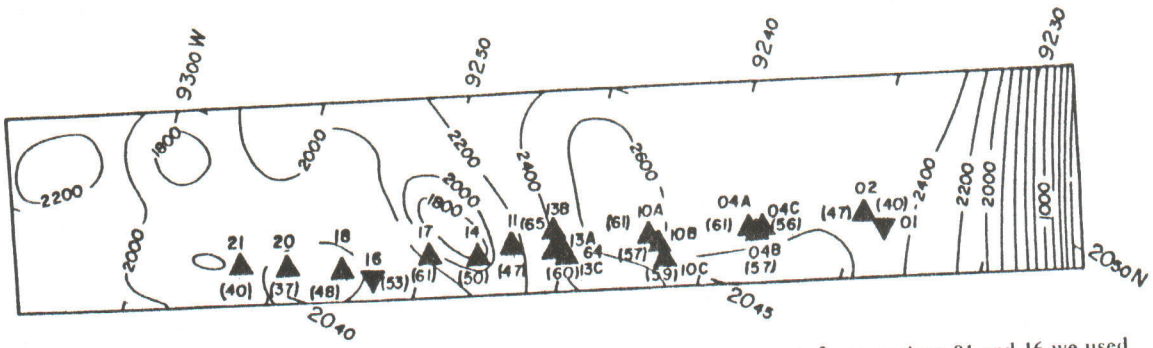


Fig. 2. Site locations for the Campeche transect and measured heat flow in mW/m$^2$. At stations 01 and 16 we used a PTG-3MTB probe. At all the other stations we used the digital thermal probe. Bathymetry contours are in meters.

tivity using two separate mineral oil-filled rods (6.0 mm diameter and 20 cm separation between them) in which thermistor sensors and heating elements are located. One rod is used for the measurements of temperature gradient. It has five sensors placed at 0.5-m intervals allowing the determination of absolute temperature with a resolution of 1 mK and temperature gradients with an instrumental error of 5 mK/m. The other rod is used for thermal conductivity measurements and has heating elements spread out the length of the rod in four 0.5-m intervals corresponding to the intervals where temperature gradient is measured by the opposite rod. In the middle of each of these intervals a temperature (heating) sensor is located (so-called "conductivity sensors"). With these sensors we obtain the integrated overall thermal conductivity much like in the needle probe method of *Von Herzen and Maxwell* [1959]. Conductive heat flow is estimated with relative errors in the 5% range between all sensor combinations.

The system samples each sensor with a 3-s sampling rate and transmits the digital multiplexed data through a three-core cable to a computer installed on board the ship. Data are demultiplexed and processed in real time by the computer which stores the data for postprocessing if necessary. Data are gathered as soon as the probe is plunged in the ocean waters.

The real-time capabilities allow the operator to sense the moment the probe penetrates the bottom sediments, where after frictional heating of the sensors ceases, he is ready to initiate the thermal conductivity measurement. During this measurement, a total of 120 data values are obtained from the moment the heating elements are activated when applying a constant current through them. The last 60 sampled points are fitted in a least squares sense to a logarithmically dependent heating curve. The in situ temperature for each sensor is obtained on the thermal gradient side of the probe. At the same time the corresponding thermal conductivity values are gathered using the other side of the probe, then the heat flow value between sensors is calculated.

At several sites, use was made of a portable thermal gradientograph (PTG-3MTB) designed by *Alexandrov* [1972] and installed on the sediment coring tube. Thermal conductivities of recovered sediments at these sites were measured in the ship's laboratory, employing the needle probe method of *Von Herzen and Maxwell* [1959] with an instrument developed by *Rot et al.* [1984].

## Measurement Results

The locations of all stations for both transects surveyed are shown in Figures 2 and 3, and the results are summarized in Table 1.

### *Campeche Transect*

Heat flow values were obtained at 18 stations on the Campeche transect on an east-west profile. Only at stations 16 and 01 were conductivities of the sediments obtained by the needle probe method; for the rest of the stations they were determined in situ. The thermal probe penetrated

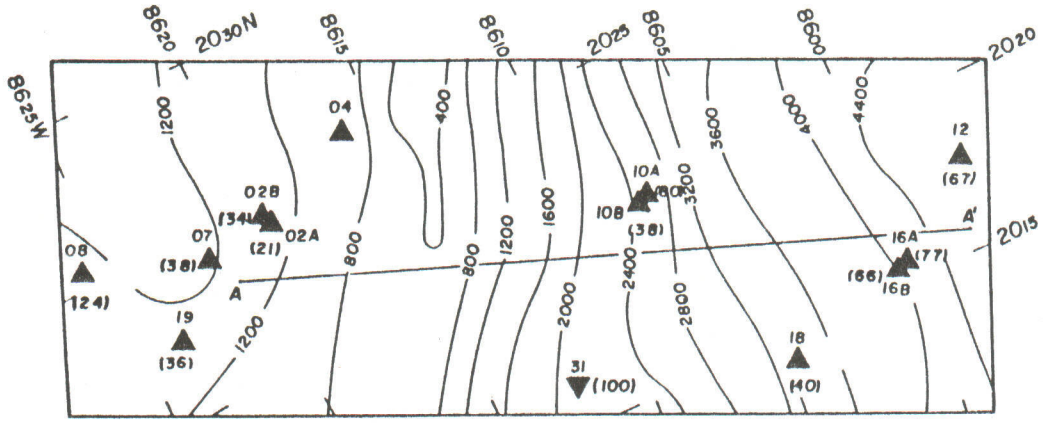


Fig. 3. Site locations for the Yucatan transect and measured heat flow in mW/m$^2$. Station 31 was obtained using the PTG-3MTB probe. Bathymetry contours are in meters.

TABLE 1. Experimental Results

| Site | Coordinates | | Depth, km | | Temperature of Bottom Sensor,* °C | Intervals Between Sensors* | | | Percent Deviation $(q_i - \bar{q})/\bar{q}$, % | Bottom Water Temperature, °C |
|---|---|---|---|---|---|---|---|---|---|---|
| | Latitude North | Longitude West | Sea Bottom | Penetration of Lower Sensor | | Temperature Gradient, mK/m | Thermal Conductivity $k$, W/mK | Heat Flow $q_i$, mW/m$^2$ | | |
| | | | | | *Campeche Transect* | | | | | |
| 01 | 20°48.7′ | 92°34.0′ | 2480 | 4.7 | | 44 | 0.908 | 40 | | 4.26 |
| 02 | 20°48.9′ | 92°34.1′ | 2453 | >2.0 | 4.321(5) | 44 | 0.901 | 39.6 | −17 | |
| | | | | | 4.343(4) | 54 | 0.918 | 49.5 | −4 | |
| | | | | | 4.3370(3) | 56 | 0.926 | 51.8 | −9 | |
| | | | | | 4.398(2) | 52 | 0.961 | 50.0 | +5 | |
| | | | | | 4.424(1) | 51.5(1–5) | 0.926(1–5) | 47.7(1–5) | | 4.29 |
| 04A | 20°47.0′ | 92°38.1′ | 2557 | >2.0 | 4.302(5) | 60 | 0.944 | 56.6 | −7 | |
| | | | | | 4.332(4) | 74 | 0.976 | 72.2 | +18 | |
| | | | | | 4.369(3) | 58 | 0.994 | 57.6 | −6 | |
| | | | | | 4.398(2) | 58 | 0.999 | 57.9 | −5 | |
| | | | | | 4.427(1) | 62.5(1–5) | 0.978(1–5) | 61.1(1–5) | | 4.29 |
| 04B | 20°47.0′ | 92°38.1′ | 2558 | >2.0 | 4.330(5) | 62 | 0.917 | 56.8 | −1 | |
| | | | | | 4.361(4) | 58 | 0.955 | 55.4 | −3 | |
| | | | | | 4.390(3) | 52 | 0.954 | 49.6 | −13 | |
| | | | | | 4.416(2) | 68 | 0.989 | 67.2 | +18 | |
| | | | | | 4.450(1) | 60(2–5) | 0.953(1–5) | 57.2(1–5) | | 4.29 |
| 04C | 20°47.1′ | 92°38.1′ | 2558 | >2.0 | 4.333(5) | 58 | 0.919 | 53.3 | −6 | |
| | | | | | 4.362(4) | 62 | 0.948 | 58.8 | −4 | |
| | | | | | 4.393(3) | 54 | 0.959 | 51.8 | −8 | |
| | | | | | 4.420(2) | 62 | 1.005 | 62.3 | −10 | |
| | | | | | 4.451(1) | 59.0(1–5) | 0.957(1–5) | 56.5(1–5) | | 4.28 |
| 10A | 20°45.1′ | 92°41.6′ | 2599 | >2.0 | 4.332(5) | 54 | 0.936 | 50.5 | −18 | |
| | | | | | 4.359(4) | 68 | 1.031 | 70.1 | +14 | |
| | | | | | 4.393(3) | 62 | 1.042 | 64.6 | +5 | |
| | | | | | 4.424(2) | 60 | 1.038 | 62.3 | +1 | |
| | | | | | 4.454(1) | 61.0(1–5) | 1.010(1–5) | 61.6(1–5) | | 4.30 |
| 10B | 20°44.9′ | 92°41.5′ | 2598 | >2.0 | 4.298(5) | 60 | 1.059 | 63.5 | +12 | |
| | | | | | 4.328(4) | 62 | 0.909 | 56.4 | −1 | |
| | | | | | 4.359(3) | 50 | 0.920 | 46.0 | −19 | |
| | | | | | 4.384(2) | 66 | 0.954 | 63.0 | +11 | |
| | | | | | 4.417(1) | 59.5(1–5) | 0.957(1–5) | 56.9(1–5) | | 4.30 |
| 10C | 20°44.8′ | 92°41.4′ | 2601 | >2.0 | 4.313(5) | 52 | 0.928 | 48.2 | −18 | |
| | | | | | 4.339(4) | 62 | 0.923 | 57.4 | −3 | |
| | | | | | 4.370(3) | 64 | 1.019 | 65.2 | +11 | |
| | | | | | 4.402(2) | 64 | 1.032 | 66.0 | +12 | |
| | | | | | 4.434(1) | 60.5(1–5) | 0.973(1–5) | 58.9(1–5) | | |

TABLE 1. (continued)

| Site | Coordinates | | Depth, km | | Temperature of Bottom Sensor,* °C | Intervals Between Sensors* | | | Percent Deviation $(q_s - \bar{q})/\bar{q}$, % | Bottom Water Temperature, °C |
|---|---|---|---|---|---|---|---|---|---|---|
| | Latitude North | Longitude West | Sea Bottom | Penetration of Lower Sensor | | Temperature Gradient, mK/m | Thermal Conductivity $k$, W/mK | Heat Flow $q_s$ mW/m$^2$ | | |
| | | | | | *Campeche Transect* (continued) | | | | | |
| 11 | 20°45.0′ | 92°45.4′ | 2397 | >2.0 | 4.321(5) | | | | | 4.28 |
| | | | | | 4.344(4) | 46 | 0.953 | 43.8 | −7 | |
| | | | | | 4.367(3) | 46 | 0.996 | 45.8 | −3 | |
| | | | | | 4.392(2) | 50 | 0.976 | 48.8 | +3 | |
| | | | | | 4.418(1) | 52 | 0.986 | 51.3 | +8 | |
| | | | | | | 48.5(1–5) | 0.978(1–5) | 47.4(1–5) | | |
| 13A | 20°44.3′ | 92°45.3′ | 2604 | >2.0 | 4.345(5) | | | | | 4.29 |
| | | | | | 4.378(4) | 66 | 0.942 | 62.2 | −3 | |
| | | | | | 4.408(3) | 60 | 0.977 | 58.6 | −8 | |
| | | | | | 4.442(2) | 68 | 0.954 | 64.9 | +1 | |
| | | | | | 4.477(1) | 70 | 1.004 | 70.3 | +10 | |
| | | | | | | 66.0(1–5) | 0.969(1–5) | 64.0(1–5) | | |
| 13B | 20°44.2′ | 92°45.2′ | 2610 | >2.0 | 4.350(5) | | | | | 4.30 |
| | | | | | 4.383(4) | 66 | 0.939 | 62.0 | −6 | |
| | | | | | 4.418(3) | 70 | 0.970 | 67.9 | +3 | |
| | | | | | 4.453(2) | 70 | 0.982 | 68.7 | +4 | |
| | | | | | 4.487(1) | 68 | 0.951 | 64.7 | −2 | |
| | | | | | | 68.5(1–5) | 0.960(1–5) | 65.8(1–5) | | |
| 13C | 20°44.1′ | 92°45.0′ | 2605 | >2.0 | 4.371(5) | | | | | 4.30 |
| | | | | | 4.403(4) | 64 | 0.930 | 59.5 | −1 | |
| | | | | | 4.431(3) | 56 | 0.992 | 55.6 | −8 | |
| | | | | | 4.464(2) | 66 | 0.962 | 63.5 | +5 | |
| | | | | | 4.497(1) | 66 | 0.943 | 62.2 | +3 | |
| | | | | | | 63.0(1–5) | 0.956(1–5) | 60.2(1–5) | | |
| 14 | 20°43.3′ | 92°48.0′ | 1626 | >2.0 | 4.249(5) | | | | | 4.21 |
| | | | | | 4.277(4) | 56 | 0.964 | 54.0 | +9 | |
| | | | | | 4.304(3) | 54 | 0.990 | 53.5 | +8 | |
| | | | | | 4.330(2) | 52 | 1.002 | 52.1 | +5 | |
| | | | | | 4.350(1) | 40 | 0.978 | 39.1 | −21 | |
| | | | | | | 50.5(1–5) | 0.983(1–5) | 49.6(1–5) | | |
| 16 | 20°42.6′ | 92°50.8′ | 2400 | 4.0 | | 58 | 0.910 | 53 | | |
| 17 | 20°41.9′ | 92°49.9′ | 2146 | >2.0 | 4.303(5) | | | | | 4.26 |
| | | | | | 4.337(4) | 68 | 0.981 | 66.7 | +8 | |
| | | | | | 4.373(3) | 72 | 0.974 | 70.1 | +14 | |
| | | | | | 4.400(2) | 54 | 0.999 | 53.9 | −12 | |
| | | | | | 4.428(1) | 56 | 0.991 | 55.5 | −10 | |
| | | | | | | 62.5(1–5) | 0.986(1–5) | 61.6(1–5) | | |

TABLE 1. (continued)

| Site | Coordinates | | Depth, km | | Intervals Between Sensors* | | | | Bottom Water Temperature, °C |
|---|---|---|---|---|---|---|---|---|---|
| | Latitude North | Longitude West | Sea Bottom | Penetration of Lower Sensor | Temperature of Bottom Sensor,* °C | Temperature Gradient, mK/m | Thermal Conductivity $k$, W/mK | Heat Flow $q$, mW/m$^2$ | Percent Deviation $(q_s - \bar{q})/\bar{q}$, % | |
| | | | | | *Campeche Transect* (continued) | | | | | |
| 18 | 20°41.3′ | 92°52.3′ | 1761 | >2.0 | 4.275(5) | | | | | 4.24 |
| | | | | | | 50 | 0.962 | 48.1 | −1 | |
| | | | | | 4.300(4) | | | | | |
| | | | | | | 50 | 0.944 | 47.2 | −3 | |
| | | | | | 4.325(3) | | | | | |
| | | | | | | 56 | 0.959 | 53.7 | +10 | |
| | | | | | 4.353(2) | | | | | |
| | | | | | | 48 | 0.952 | 45.7 | −6 | |
| | | | | | 4.377(1) | | | | | |
| | | | | | | 51.0(1–5) | 0.954(1–5) | 48.6(1–5) | | |
| 20 | 20°41.4′ | 92°54.8′ | 1744 | >2.0 | 4.271(5) | | | | | 4.23 |
| | | | | | | 30 | 0.965 | 29.0 | −22 | |
| | | | | | 4.286(4) | | | | | |
| | | | | | | 42 | 0.988 | 41.5 | +12 | |
| | | | | | 4.307(3) | | | | | |
| | | | | | | 50 | 0.972 | 48.6 | +31 | |
| | | | | | 4.332(2) | | | | | |
| | | | | | | 30 | 0.979 | 29.4 | −21 | |
| | | | | | 4.347(1) | | | | | |
| | | | | | | 38.0(1–5) | 0.976(1–5) | 37.1(1–5) | | |
| 21 | 20°41.1′ | 92°56.3′ | 1883 | >2.0 | 4.274(5) | | | | | 4.24 |
| | | | | | | 48 | 0.978 | 46.9 | +18 | |
| | | | | | 4.298(4) | | | | | |
| | | | | | | 34 | 0.992 | 33.7 | +15 | |
| | | | | | 4.315(3) | | | | | |
| | | | | | | 42 | 0.993 | 41.7 | +4 | |
| | | | | | 4.337(2) | | | | | |
| | | | | | | 36 | 0.976 | 35.1 | −12 | |
| | | | | | 4.355(1) | | | | | |
| | | | | | | 40.5(1–5) | 0.985(1–5) | 39.9(1–5) | | |
| | | | | | *Yucatan Transect* | | | | | |
| 02A | 20°24.9′ | 86°19.5′ | 1213 | >2.0 | 4.258(5) | | | | | 4.44 |
| | | | | | | 2 | 0.970 | 1.9 | | |
| | | | | | 4.459(4) | | | | | |
| | | | | | | 14 | 0.957 | 13.4 | † | |
| | | | | | 4.466(3) | | | | | |
| | | | | | | 20 | 1.025 | 20.5 | † | |
| | | | | | 4.476(2) | | | | | |
| | | | | | | 32 | 0.998 | 31.9 | † | |
| | | | | | 4.492(1) | | | | | |
| | | | | | | 22.0(1–4) | 0.987(1–5) | 21.7(1–4) | | |
| 02B | 20°25.0′ | 86°19.8′ | 1217 | >2.0 | 4.261(5) | | | | | 4.44 |
| | | | | | | −10 | 1.014 | −10.1 | | |
| | | | | | 4.456(4) | | | | | |
| | | | | | | 34 | 1.019 | 34.6 | † | |
| | | | | | 4.473(3) | | | | | |
| | | | | | | 30 | 1.021 | 30.6 | † | |
| | | | | | 4.488(2) | | | | | |
| | | | | | | 38 | 1.013 | 38.5 | † | |
| | | | | | 4.507(1) | | | | | |
| | | | | | | 34.0(1–4) | 1.017(1–5) | 34.6(1–4) | | |
| 04 | 20°26.2′ | 86°16.2′ | 1099 | >2.0 | 4.703(5) | | | | | 4.68 |
| | | | | | | −18 | 1.104 | −19.9 | | |
| | | | | | 4.694(4) | | | | | |
| | | | | | | −14 | 1.094 | −15.3 | † | |
| | | | | | 4.687(3) | | | | | |
| | | | | | | 0 | 1.128 | 0 | † | |
| | | | | | 4.687(2) | | | | | |
| | | | | | | 0 | 1.160 | 0 | † | |
| | | | | | 4.687(1) | | | | | |
| | | | | | | | 1.121(1–5) | | | |

TABLE 1. (continued)

| Site | Coordinates | | Depth, km | | Temperature of Bottom Sensor,* °C | Intervals Between Sensors* | | | Percent Deviation $(q_s - \bar{q})/\bar{q}$, % | Bottom Water Temperature, °C |
|---|---|---|---|---|---|---|---|---|---|---|
| | Latitude North | Longitude West | Sea Bottom | Penetration of Lower Sensor | | Temperature Gradient, mK/m | Thermal Conductivity $k$, W/mK | Heat Flow $q_s$, mW/m$^2$ | | |
| | | | | | *Yucatan Transect* (continued) | | | | | |
| 07 | 20°24.5′ | 86°21.7′ | 1195 | >2.0 | 4.469(5) | | | | | 4.34 |
| | | | | | 4.463(4) | −12 | 1.066 | −12.8 | | |
| | | | | | 4.480(3) | 34 | 1.064 | 36.2 | −6 | |
| | | | | | 4.500(2) | 40 | 1.033 | 41.3 | +7 | |
| | | | | | 4.517(1) | 34 | 1.118 | 38.0 | −1 | |
| 08 | 20°25.6′ | 86°25.7′ | 1201 | >2.0 | 4.473(5) | 36.0(1–4) | 1.069(1–5) | 38.5(1–4) | | 4.38 |
| | | | | | 4.473(4) | 0 | 1.040 | 0 | | |
| | | | | | 4.481(3) | 16 | 1.038 | 16.6 | −32 | |
| | | | | | 4.494(2) | 26 | 1.047 | 27.2 | +12 | |
| | | | | | 4.508(1) | 28 | 1.067 | 29.2 | +22 | |
| 10A | 20°20.5′ | 86°07.7′ | 2760 | >2.0 | 4.209(5) | 23.3(1–4) | 1.048(1–5) | 24.4(1–4) | | 4.13 |
| | | | | | 4.246(4) | 74 | 0.957 | 70.8 | +17 | |
| | | | | | 4.278(3) | 64 | 0.978 | 62.6 | +3 | |
| | | | | | 4.307(2) | 58 | 0.981 | 56.1 | −7 | |
| | | | | | 4.334(1) | 54 | 0.957 | 51.7 | −14 | |
| 10B | 20°20.4′ | 86°08.0′ | 2760 | >1.5 | 4.157(4) | 62.5(1–5) | 0.968(1–5) | 60.6(1–5) | | 4.13 |
| | | | | | 4.206(3) | 98 | 1.313 | 128.7 | −7 | |
| | | | | | 4.265(2) | 118 | 1.324 | 156.2 | +13 | |
| | | | | | 4.331(1) | 132 | 1.007 | 132.9 | −4 | |
| 12 | 20°17.2′ | 85°56.5′ | 4511 | >2.0 | 4.202(5) | 116.0(1–4) | 1.195(1–4) | 138.6(1–4) | | 4.36 |
| | | | | | 4.439(4) | 74 | 1.082 | 80.1 | +19 | |
| | | | | | 4.471(3) | 64 | 1.078 | 69.0 | +2 | |
| | | | | | 4.497(2) | 52 | 1.049 | 54.5 | −19 | |
| | | | | | 4.530(1) | 66 | 0.998 | 65.9 | −2 | |
| 16A | 20°15.6′ | 85°59.8′ | 4002 | >2.0 | 4.343(5) | 64.0(1–5) | 1.051(1–5) | 67.3(1–5) | | 4.30 |
| | | | | | 4.379(4) | 72 | 0.999 | 71.9 | −7 | |
| | | | | | 4.420(3) | 82 | 1.028 | 84.3 | +9 | |
| | | | | | 4.454(2) | 68 | 1.062 | 72.2 | −7 | |
| | | | | | 4.494(1) | 78 | 1.027 | 80.1 | +3 | |
| 16B | 20°15.4′ | 86°00.1′ | 3967 | >2.0 | 4.342(5) | 75.5(1–5) | 1.028(1–5) | 77.6(1–5) | | 4.30 |
| | | | | | 4.371(4) | 58 | 1.044 | 60.5 | −9 | |
| | | | | | 4.408(3) | 74 | 1.046 | 77.4 | +16 | |
| | | | | | 4.437(2) | 58 | 1.080 | 62.6 | −5 | |
| | | | | | 4.466(1) | 58 | 1.112 | 64.5 | −3 | |
| | | | | | | 62.0(1–4) | 1.069(1–5) | 66.3(1–5) | | |

TABLE 1. (continued)

| Site | Coordinates: Latitude North | Coordinates: Longitude West | Depth, km: Sea Bottom | Depth, km: Penetration of Lower Sensor | Temperature of Bottom Sensor,* °C | Intervals Between Sensors*: Temperature Gradient, mK/m | Intervals Between Sensors*: Thermal Conductivity $k$, W/mK | Intervals Between Sensors*: Heat Flow $q$, mW/m$^2$ | Percent Deviation $(q_s - \bar{q})/\bar{q}$, % | Bottom Water Temperature, °C |
|---|---|---|---|---|---|---|---|---|---|---|
| | | | | | *Yucatan Transect* (continued) | | | | | |
| 18 | 20°14.2′ | 86°04.6′ | 3267 | >1.5 | 4.207(4) | | | | | 4.20 |
| | | | | | | 34 | 1.021 | 34.7 | −13 | |
| | | | | | 4.224(3) | | | | | |
| | | | | | | 32 | 0.999 | 32.0 | −20 | |
| | | | | | 4.240(2) | | | | | |
| | | | | | | 50 | 1.076 | 53.8 | +35 | |
| | | | | | 4.265(1) | | | | | |
| | | | | | | 38.7(1–4) | 1.031(1–4) | 39.9(1–4) | | |
| 19 | 20°22.3′ | 86°23.5′ | 1204 | >2.0 | 4.364(5) | | | | | 4.37 |
| | | | | | | 0 | 1.012 | 0 | | |
| | | | | | 4.464(4) | | | | | |
| | | | | | | 22 | 1.017 | 2 | −38 | |
| | | | | | 4.475(3) | | | | | |
| | | | | | | 38 | 1.061 | 40.3 | +11 | |
| | | | | | 4.494(2) | | | | | |
| | | | | | | 46 | 1.033 | 47.5 | +30 | |
| | | | | | 4.517(1) | | | | | |
| | | | | | | 35.3(1–4) | 1.030(1–5) | 36.4(1–4) | | |
| 31‡ | 20°16.8′ | 86°12.0′ | 2180 | 4.3 | | 101 | 0.990 | 100 | | |

*Numbers in parentheses refer to lower (1) to upper (5) sensors.
†Influence of exogenuous thermal wave.
‡Measurements of gradient by PTG-3MTB, $k$ values with needle-probe technique aboard ship.

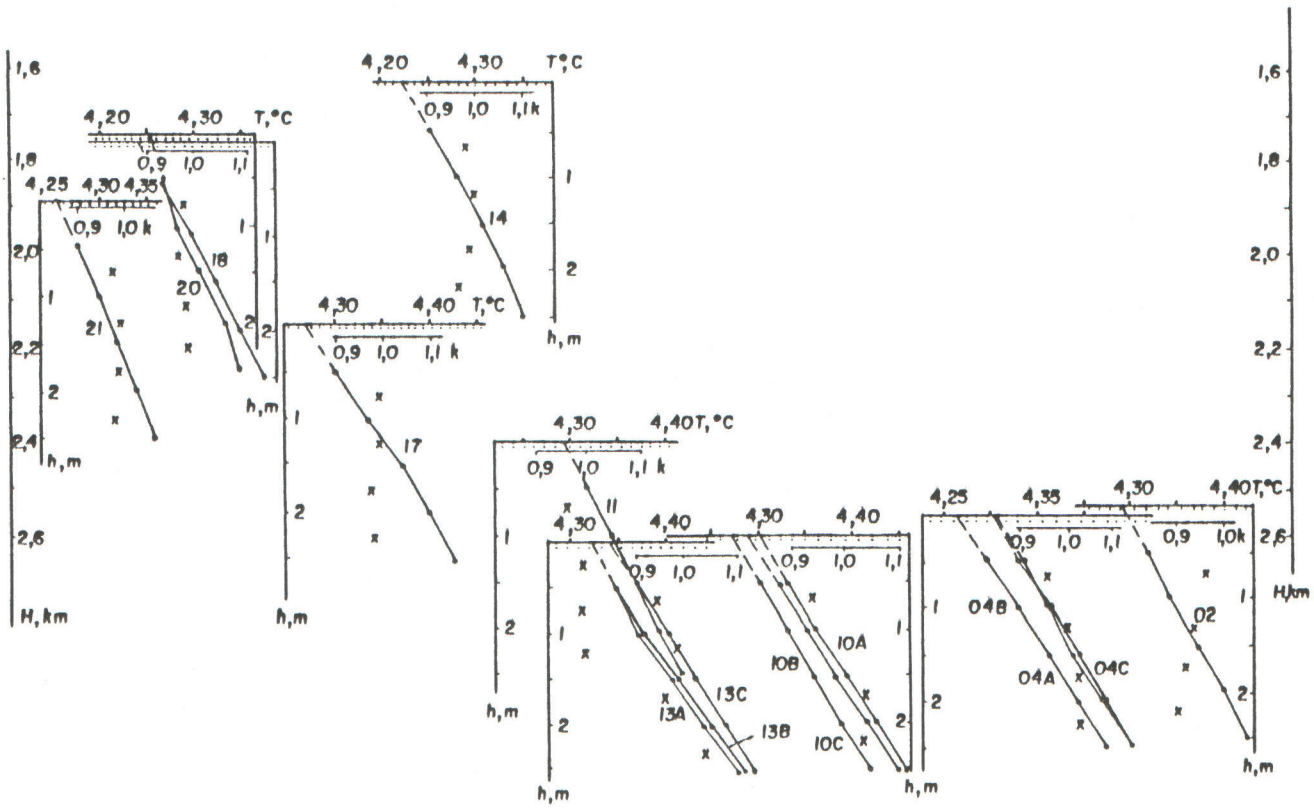


Fig. 4. Measurement results using the digital probe in the Campeche transect. The temperature axis coincides with the bottom depth $H$. For each station we show plots of temperature versus depth of probe penetration $h$ and thermal conductivity $k$ in W/mK (measured in situ) denoted with a cross. Points correspond to the position of heating temperature sensors.

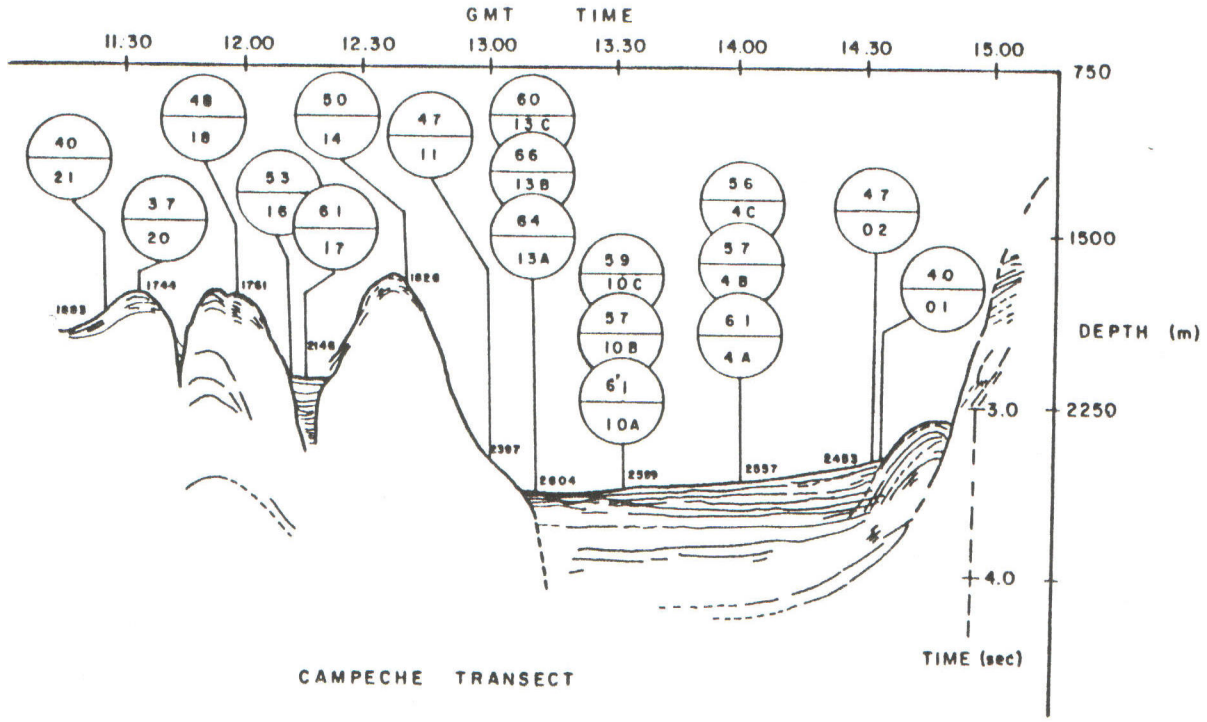


Fig. 5. Tracing of seismic section along the Campeche transect with site locations and measured heat flow in $mW/m^2$. Depths to bottom are those obtained from single-channel echo sounding at the time of penetration.

completely into the bottom sediments at all of these sites. This has permitted us to draw conclusions about the variability in geothermal parameters within the sediments.

In this area we obtained thermal conductivities within the range of 0.901–1.042 W/mK. The overall average was $\bar{k}$ = 0.97 ± 0.02 W/mK, yielding a standard deviation of $\sigma_{\bar{k}}$ = ± 0.036. Individual station averages stayed within $3\sigma_{\bar{k}}$ from the mean $\bar{k}$.

In Figure 4 we have summarized the results for sites in the Campeche transect where the digital thermal probe was used. Absolute bottom temperature and thermal conductivity are plotted as a function of oceanic depth $H$ and the estimated depth $h$ of measurement within the sediments obtained from the in situ temperature gradients. There is an almost linear relation between temperature versus depth $h$ in the sediments. In the salt dome area, where rugged topography is present, the thermal gradient shows slightly larger variations from the mean. However, the heat flow values remain relatively constant throughout the probes entire length.

In Figure 5 we show the tracing of the seismic profile for the Campeche transect, with a general interpretation of the observations. Station average heat flow values and depths to the sea bottom, obtained from single-channel echo sounding at the time of penetration, are also shown. Interesting features on the seismic section are worth discussing in connection with the heat flow data.

To the west we distinguish on the seismic section several structures associated with the area of domes and knolls defined by *Worzel et al.* [1968]. Sedimentary thicknesses here seem quite uniform, consisting mainly of terrigeneous sediments and evaporites. To the east the basin is filled with sediments showing almost horizontal stratification except near the eastern scarp where there is evidence of slumping from the continental shelf (Campeche Bank). This sedimentary sequence has a 200-m seafloor relief difference dipping to the west, probably as a result of the high rate of sediment contribution from the continental shelf.

At first sight the observed heat flow values differ somewhat between the western (Salt Dome Province) and eastern parts of the section (Campeche Canyon). On the west, the average heat flow is 48 ± 7 $mW/m^2$ and on the east has an average value of 58 ± 6 $mW/m^2$. However, when we ran a nonparametic Wilcoxon rank-sum test [*Bhattacharyya and Johnson*, 1977] to the two data sets, we obtained small levels of significance supporting shifted population distributions. Thus, from a statistical point of view, a 53.7 $mW/m^2$ average heat flow with a standard deviation of ±8.5 $mW/m^2$ will be assumed for the entire Campeche transect. This average heat flow would be less than that derived from the mantle below if high rates of sedimentation persisted during long periods of time in the area. However, from a qualitative analysis of individual heat flow stations for this transect, we believe that these data are influenced by the variability in sea bottom relief present in the area, with other environmental factors having lesser influence upon them.

From the work of *Worzel et al.* [1968], *Epp et al.* [1970], and primarily from the cores recovered during our study and the results of *Deep Sea Drilling Project* (DSDP) [1973] leg 10 (drilling sites 87, 85, and 88), rates of sediment deposition can be estimated for the NE Campeche Canyon and the Salt Dome Province. These are summarized as follows: (1) sediment deposition was highest in the entire Gulf of Mexico during Pleistocene time, with estimated rates around 3–4 cm/1000 years for the Salt Dome Province and between 2 and 10 cm/1000 years near the Campeche Scarp, northeast from the Campeche Canyon, (2) during Pliocene times, the entire gulf was subjected to sediment rates of 2–4 cm/1000 years,

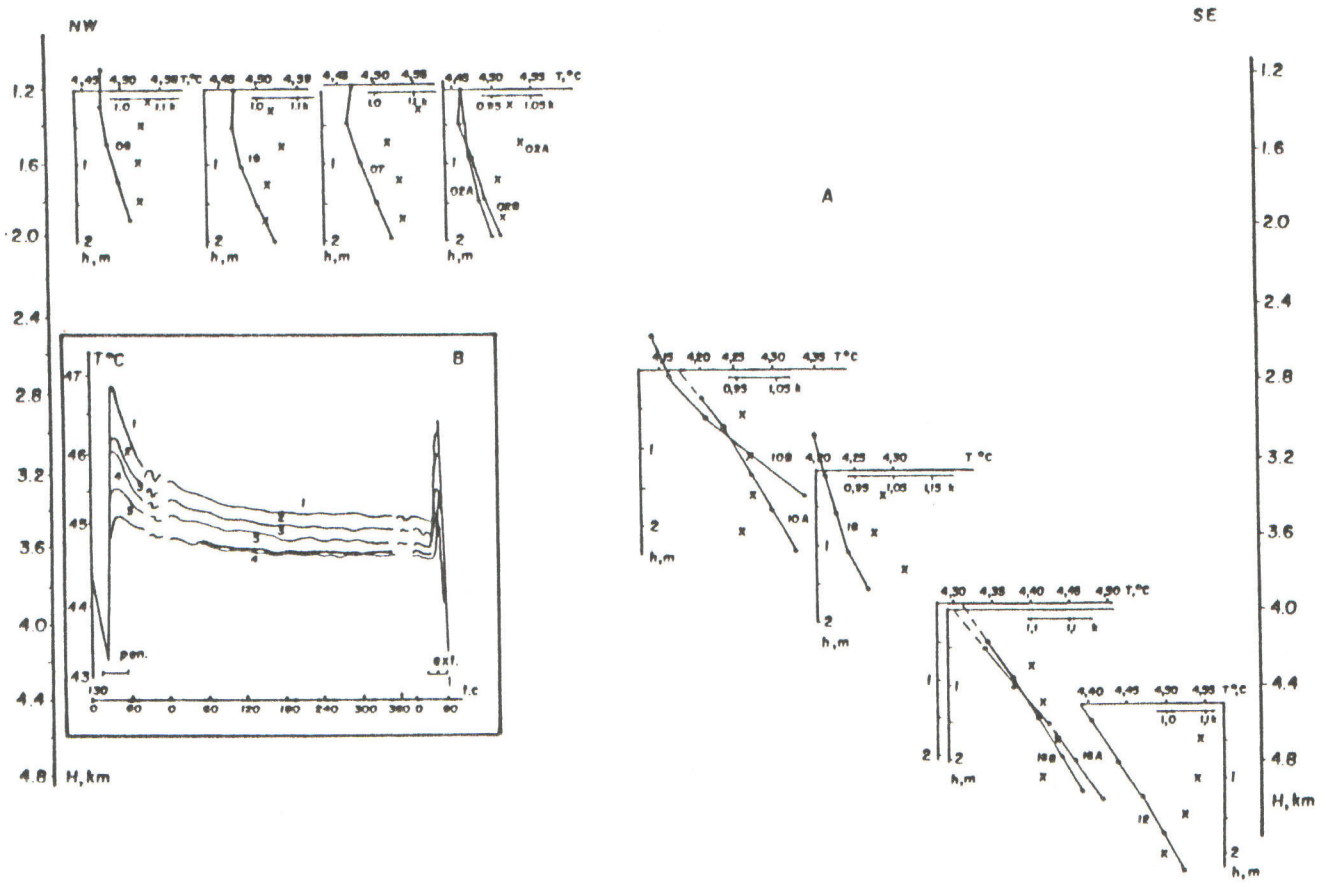


Fig. 6. Measurements results for the Yucatan transect (*a*) same as Figure 4 and (*b*) temperature $T$ at station 07 from the lower (1) to the upper (5) sensors versus measuring time $t$; "pen" and "ext" stand for the moment of penetration and extraction of the probe, respectively.

and (3) in the upper Miocene, rates decreased to 1 cm/1000 years on the Campeche Scarp, northeast from the Campeche Canyon, diminishing (backward in time) in the early Tertiary to 0.5 cm/1000 years.

In Campeche Canyon, most recovered sediments showed strong mixing from turbidity currents and slumping of terrigenous material from the Campeche Bank. Sediment thicknesses inferred from our seismic data to acoustic basement exceed 1.8 km (velocity of 2.5–2.7 km/s) which, according to *Smith and McNeely*'s [1973] biostratigraphic cross section for the gulf, comprises Pleistocene, Pliocene, and Miocene age sediments.

In the Salt Dome Province the sediments recovered were pelagic in nature, deposited at least since middle Pliocene, with small amounts of terrigenous derived material, transported by turbiditic currents. Here, sediment thicknesses do not exceed 500 m.

When correlating rates of deposition for the last 10 m.y. and thickness of sediments with heat flow [*Von Herzen and Uyeda*, 1973; *Hutchison*, 1985], we found less than 20% expected reduction in heat flow for the Campeche Canyon and 5% in the Salt Dome Province. The latter reducing factor is within our experimental error and hence will not be applied to our data. Concerning the Campeche Canyon, our uncorrected data already show higher than average heat flow as compared with data from North Atlantic basins. Only stations 01 and 02, near the Campeche Scarp, show lower than average values, and these data may be affected by variable rates of deposition which are difficult to estimate due to slumping.

It has been much more difficult to estimate other environmental factors affecting our data, such as pore fluid circulation or fluctuations in bottom temperatures [*Langseth et al.*, 1966; *Wang and Beck*, 1987]. Reliable hydrographic data at the scale of our detailed study that could be correlated to changes in bottom temperatures are not available.

In summary, from a qualitative analysis of our data, high heat flow is apparent within the closed-in basin forming the Campeche Canyon, which goes against what one would expect from high rates of sedimentation. The same can be said for station 17, located in a small deep flanked by knolls and located in the Salt Dome Province (see Figure 5). Also, lower than average heat flow was observed for stations located on flanks or topographic highs. All these lead us to conclude that our raw data for this transect show typical response from surface effects. Under this premise and bearing in mind our difficulties in estimating the effects of other environmental factors, we have preferred to conduct a two-dimensional forward modeling in order to evaluate thermal refraction effects and contrasts in thermal properties, from the geologic section, on the raw data.

From the thermal sounding of the water column in this area we found that in situ water temperature decreases with depth down the bottom to 4.21°C at near 1600 m. Below this level it increases with a 90 mK/m gradient. This in situ temperature distribution is considered typical for closed-in

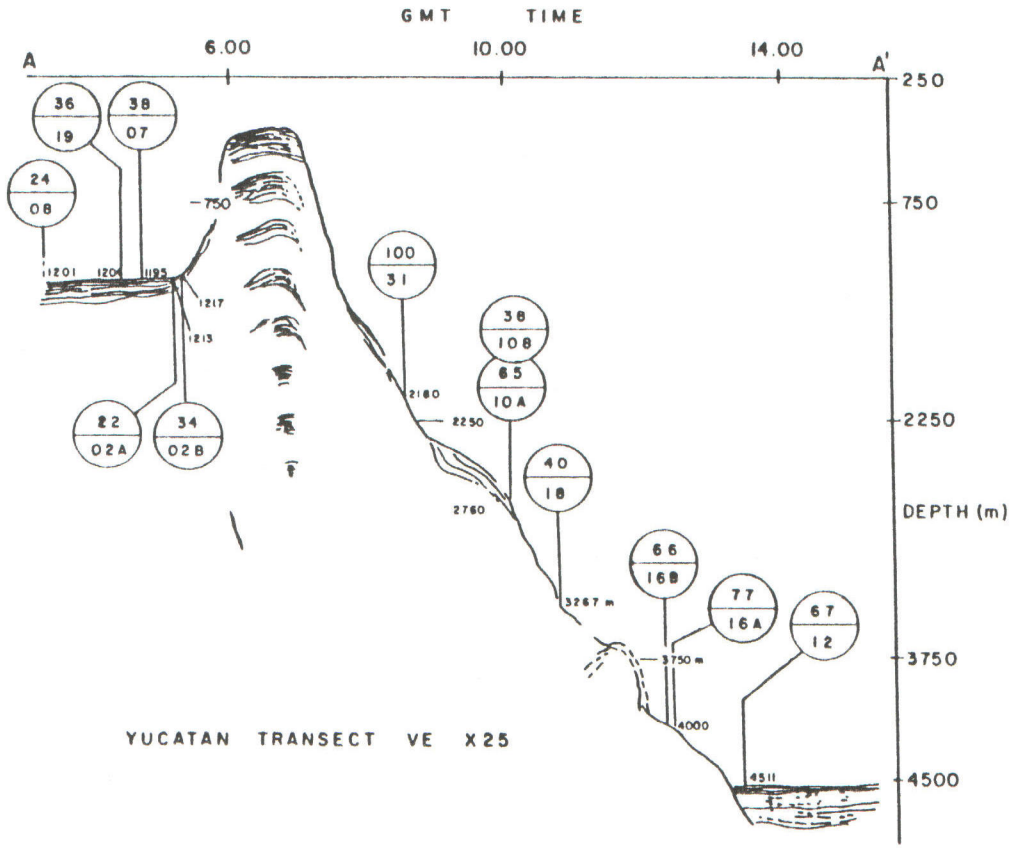


Fig. 7. Tracing of seismic section along profile AA' of Figure 3 for the Yucatan transect. Site locations shown in Figure 3 were projected onto this profile for clarity. Heat flow values are in $mW/m^2$.

oceanic basins as contrasted to that found in abyssal plains. These data allowed us to set the upper boundary condition for modeling at a temperature of 4.2°C.

*Yucatan Transect*

The results for the Yucatan transect were plotted in the same fashion as for the Campeche area and are shown in Figure 6. Thirteen stations were surveyed in the upper and lower basins and in the local depression on the continental slope. At all stations we used the digital thermal probe, except at station 31. In only three instances the top thermal sensor remained outside the sediments (this is clearly shown in Figure 6*a*). Thermal conductivity was measured in situ at 11 stations, while at two others it was estimated from the recovered sediments using the needle probe method. We found that thermal conductivities do not vary spatially in a systematic manner as was the case for the Campeche transect.

The average thermal conductivity for the whole Yucatan survey was $\bar{k} = 1.046$ W/mK and $\sigma_{\bar{k}} = \pm 0.06$. We did not estimate the heat flow over the small uplift section separating the basin because of the likely influence of nonstationary temperatures at such shallow depths. We found, furthermore, that this effect tends to predominate even at greater depth as evidenced in the data obtained for the upper basin. Station 04, at a depth of 1099 m, shows a negative heat flow value (see Table 1). At some other stations, heat flow values in between the uppermost sensors were near zero as well (see Figure 6*a* and Table 1). In all of these cases, however, as shown by the recorded temperature curves for station 07 (Figure 6*b*), the upper sensor was well into the sediments. These data show exogeneous temperature effects in the upper basin (and probably not only here), traced down to a water depth of 1200 m.

On the continental slope the depth of measurements exceeded 2 km with no clear evidence of exogeneous effects. Heat flow values excluding stations 10B and 31 are, in general, higher here (average of 62.2 ± 12 $mW/m^2$) than on the upper basin (average of 31.1 ± 6.7 $mW/m^2$ using the lower sensors of the thermal probe). Two particularly high heat flow values (100 and 139 $mW/m^2$) were obtained half way down the slope associated with a fault, previously detected by a seismic survey.

In Figure 7 we show the tracing of seismic profile AA' of Figure 3 with a general interpretation of the observations. Stations have been projected onto this profile for clarity. Heat flow stations 08, 19, 07, 02A, and 02B are located on the upper basin; the rest are situated downslope toward the Yucatan basin.

From the work of *Erickson et al.* [1972], average rates of sediment deposition for the Yucatan basin since Eocene times may be less than 1 cm/1000 years. For the upper basin these rates are not known well enough. However, from cores recovered in our study, sediments in the upper basin are mainly constituted of clay turbidites with little traces of terrigenous components in them, similar to those obtained for the lower Yucatan basin. This same acoustically opaque turbidite material is inferred from seismics to be present at

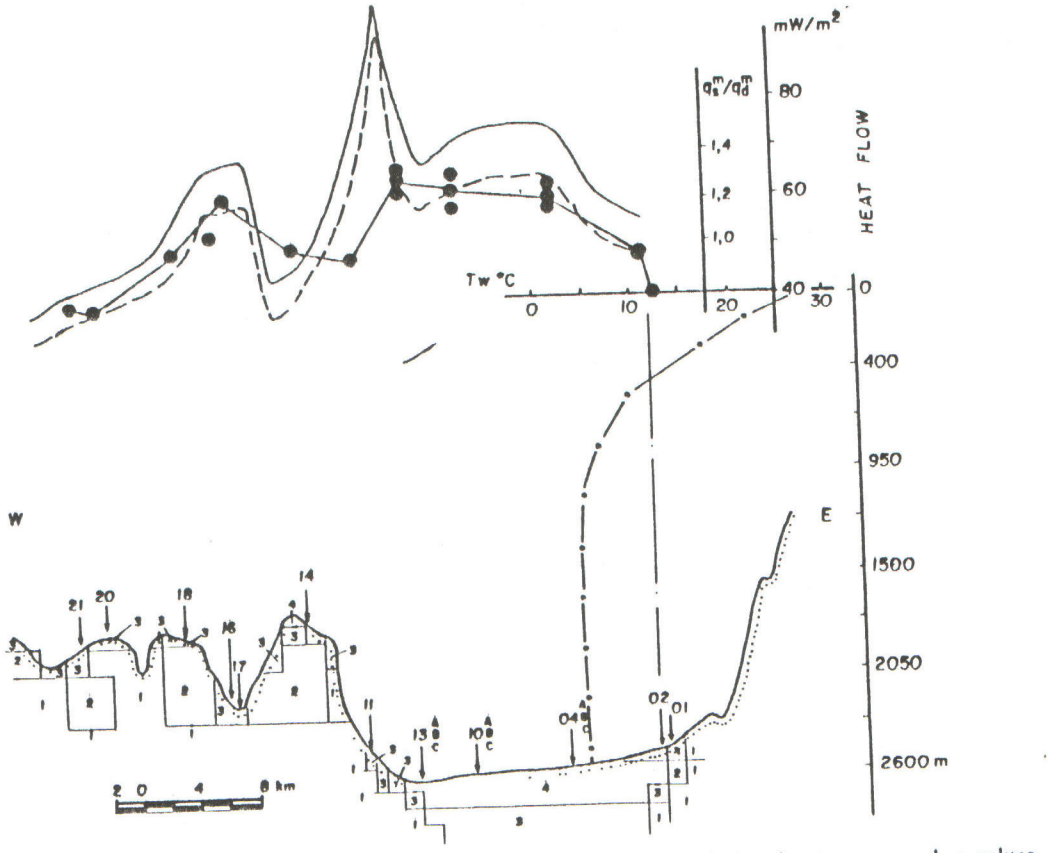


Fig. 8. Results of heat flow modeling for the Campeche transect. Solid circles denote measured $q$ values, continuous curve denotes $q_s^m$ modeled, and dotted curve denotes relative $q_s^m/q_d^m$ values. At station 02 we show the seawater temperature $T_w$ versus depth $H$. The discretization of the upper part of the model is shown with thermal conductivities used. These are (1) carbonate-terrigenous acoustic basement, $k$ = 2.5 W/mK, (2) evaporites, $k$ = 3.5 W/mK, (3) terrigenous sediments of the dome area and the lower part of the sedimentary cover in the Campeche Canyon, $k$ = 1.8 W/mk, and (4) terrigenous sediments of the upper part of the sedimentary cover in the Campeche Canyon, $k$ = 1.0 W/mk.

both basins, suggesting that recent sedimentary deposition for the upper basin may equal that for the Yucatan basin. This low rate of sedimentation will cause the measured gradients to be about 95% of the undisturbed regional gradient. The inflow of Atlantic deep water through known passages may have produced changes in bottom water temperatures in the Caribbean Sea and particularly in the upper basin of Yucatan peninsula. However, as in the Gulf of Mexico there are little data available from which to estimate corrections due bottom water temperature fluctuations for this transect.

The bottom water temperature as a function of depth $H$ in this area reaches a minimum of 4.13°C at 2700 m and increases from there on at a rate of about 130 mK/m. On the average, we found a terminal temperature at depth in the range 4.3°–4.4°C. The value of 4.3°C was used as an upper boundary condition for modeling.

## Modeling

Individual heat flow values, measured at the ocean bottom, can show marked variations due to topographic features, sedimentation, fluctuations in bottom water temperature, circulation of pore fluids, and/or inherent contrast in thermal properties between geological bodies comprising crustal section and henceforth, making it difficult to estimate the background heat flow. A two-dimensional conductive modeling of heat flow for the studied areas was performed in order to estimate quantitatively the influence of seafloor relief [*Henry and Pollack*, 1985] and contrasting thermal properties of the assumed crustal section.

The initial model for each transect was estimated by solving the one-dimensional heat transfer equation without internal sources for each station and using the following information: (1) bottom topography obtained from ECHOS multibeam bathymetric charts [*De Moustier*, 1988], (2) morphology of the elements pertaining to the geological sections with differing thermal properties, (3) single-channel seismic profiling to estimate the "roof" of evaporites in the Campeche transect and acoustic basement in the case of the Yucatan transect, (4) thermal conductivities for the sediments, based on our measurements, and for rock salt and acoustic basement from published data [*Haenel et al.*, 1988], and (5) absolute temperature at the upper boundary of the modeled region (i.e., at the seafloor) from our thermal sounding data.

From these one-dimensional models we estimated the depth and temperature of the lower isotherm (lower boundary condition) used in the two-dimensional modelling case. The depth chosen corresponds to that level where this isotherm can safely be assumed to be horizontal for the

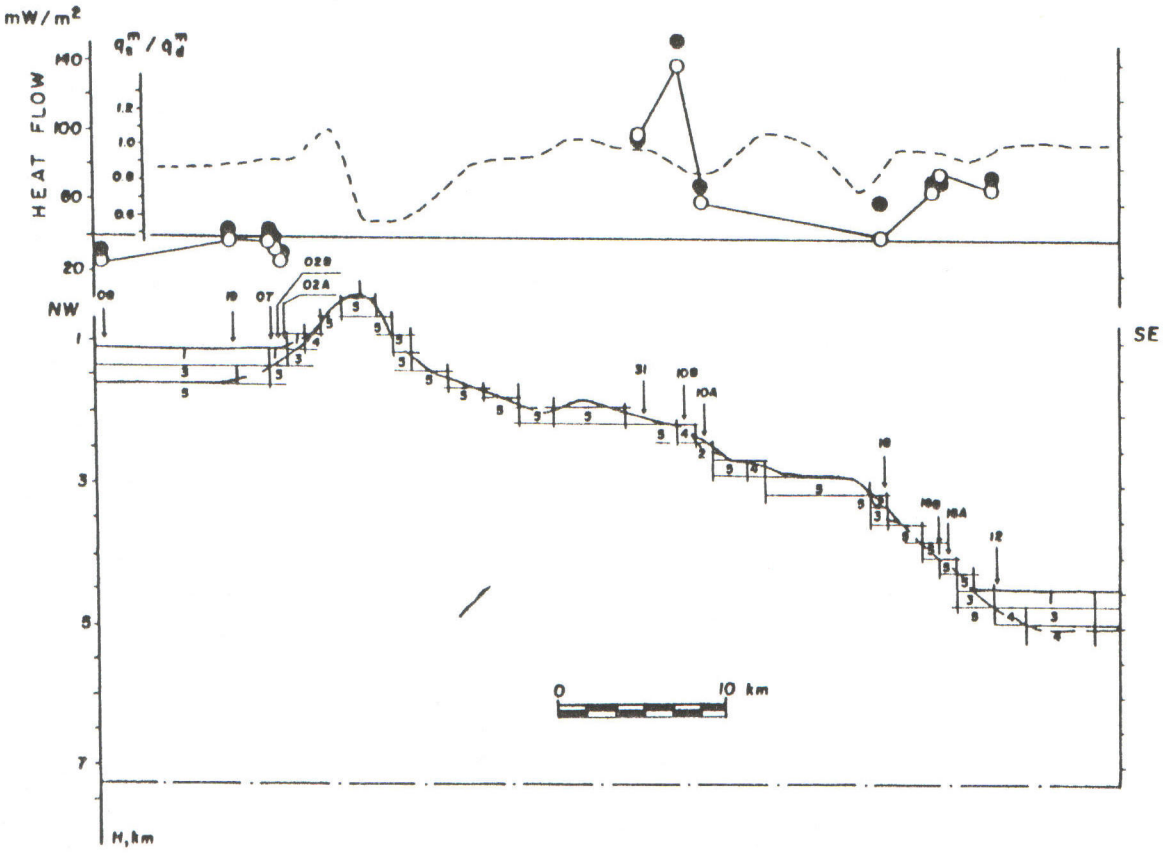


Fig. 9. Measurements results for the Yucatan transect. Open circles are heat flow values $q_s$ measured, solid circles are corrected for refraction $q_s^m$, and dashed curve is relative values of heat flow $q_s^m/q_d^m$ from the model. The discretization for the model is shown where the different conductivities are (1) $k$ = 1.0 W/mk, (2) $k$ = 1.3 W/mk, (3) $k$ = 1.8 W/mk, (4) $k$ = 2.1 W/mk, and (5) $k$ = 2.5 W/mK. See explanation in the text.

length of the transect or portions of it. For the Campeche transect this isotherm was placed the length of the survey line at 3 km depth from the highest seafloor relief found in the Salt Dome Province, where the one-dimensional response shows constant temperature of 125°C at this depth. For the Yucatan transect the one-dimensional model required two horizontal isotherms, both at a depth of 2.75 km below the sea bottom in the Yucatan basin but with different temperatures, one for the western end at 116°C and one for the eastern end at 65°C, with a smooth interpolation inbetween.

The temperature distribution and heat flow were estimated using a finite element code, kindly provided to us by N. A. Pal'shin. The code yields the modeled heat flow values at the oceanic bottom surface ($q_s^m$) together with the ratio $q_s^m/q_d^m$ (where $q_d^m$ is the modeled "deep" heat flow value which is free from the surface effects) and that found at the same depth where initial boundary conditions were imposed. This ratio reflects the contrasting properties in thermal conductivity of the overlaid stratum. These theoretical values are then compared to those obtained experimentally in order to determine true deep heat flow values at all sites.

## Discussion

The heat flow measurements that we made west from the Campeche Bank are the first reported in this part of the Gulf of Mexico. Most of the earlier heat flow data are associated with the Central Gulf, i.e., the Sigsbee abyssal plain and its northern fringes, in particular, the Mississippi trough and submarine fan [*Epp et al.*, 1970].

These data have shown an average heat flow through the gulf of 35 mW/m$^2$. One exception is the Sigsbee ridge, in the plain of the same name, with relatively high heat flow of between 52 and 91 mW/m$^2$. These high values have been attributed to an effect of mass heat transfer associated with rapid growth of salt domes in the area.

The results from the Yucatan transect have increased our knowledge on the geothermal condition in the Yucatan basin of Caribbean Sea. In this basin the first six sites yielded heat flow values in the range of 54–75 mW/m$^2$ [*Epp et al.*, 1970; *Rosencrantz et al.*, 1989]. The next three sites in this depression showed homogeneous average values of 61 mW/m$^2$ [*Erickson et al.*, 1972; *Rosencrantz et al.*, 1989]. Our data do agree quite well with these previous results.

### *Campeche Transect*

Concerning our Campeche transect data, we found a slight increase in heat flow within the Canyon as compared to the neighbouring Salt Dome Province. *Antoine and Pyle* [1970] believe that in this transect a sedimentary cover conceals the presence of a deep fault which separates blocks of different crustal thicknesses. Henceforth, as a result of fault controlled thermal activity, an increase in heat flow in the canyon can be expected. This inference may be valid for the

Sigsbee ridge; however, our data do not fully support this for the case of the Campeche Canyon. In fact, the heat flow distribution in the Campeche area reflects the influence of topographic effects, partly compensated by contrasting thermal conductivities of sediments and evaporites. This was corroborated by two-dimensional modeling of the area. The modeling yielded a distribution of heat flow along the ocean bottom surface $q_s^m$ and the ratio $q_s^m/q_d^m$, shown in Figure 8. We see that the overall distribution of observed heat flow is quite similar to the theoretical results and also the estimated average "deep" heat flow within the transect is rather uniform, with a value of 51 mW/m$^2$ and a ±5 standard deviation (half the standard deviation of the experimental data). Hence we can postulate that variations in heat flow for this area are controlled mainly by the relief in the oceanic bottom surface.

This is an important result, which leads us to conclude that the thermal regime in the Salt Dome Province of the Gulf of Mexico, where halokinesis takes place, is influenced by topographic features. The rate of erosion of submarine relief is much slower than that on land. Subareal halokinetic regions are usually peneplanated (e.g., North Caspian, North German depressions, etc.), and the salt diapirs are directly responsible for the anomalous heat flow values, but topography does not influence them.

### *Yucatan Transect*

In the Yucatan transect we wanted to estimate how much our heat flow data reflected the geological heterogeneities of the area as well as the influence of its bottom topography. For this purpose, we followed a similar approach to the one used in modeling the Campeche area.

In order to construct a reasonable heat flow model we used six different thermal conductivity values attributed to different structural bodies in accordance with their real and assumed constitution (water content, lithology, etc.): (1) 1.0 W/mK for the uppermost part of bottom sediments (according to our measurements), (2) 1.3 W/mK for their lower part, (3) 1.8 W/mK for the lowest part of sediments, (4) 2.1 W/mK for the transition zone between sediments and acoustic basement, and (5) 2.5 W/mK for this basement (value corresponding to limestones and amphibolite shales).

The temperatures from numerical modeling for the entire area allowed us to estimate the ratio ($\mu$) of the surface heat flow ($q_s^m$) to the "deep" one ($q_d^m$). The "deep" heat flow was calculated from $q_d^m = q_s^m/\mu$ (Figure 9). These values are 38 ± 5 mW/m$^2$ for the "upper" basin and 69 ± 5 mW/m$^2$ for the "lower" basin. A nonparametric Wilcoxon rank-sum test proved heterogeneity in the "upper" and "lower" basins in $q$ values with the exception of two anomalously high values 96 and 115 mW/m$^2$. Thus differences of heat flow in the "upper" and "lower" basins are not compensated only by the influence of bottom topography and structure of the geological sequence. Apparently, these differences are of a different nature. Unequal depths of thermal sources under lithosphere blocks of different age may be regarded as possible cause of this heterogeneities. We cannot rule out the possible effects of bottom water temperature fluctuations, particularly for the "upper" shallower basin, where the lack of hydrographic data precludes any estimation of appropriate correction factors in our data.

Anomalously high heat flow values in the middle of the continental slope (stations 10B and 31) are apparently the result of convective heat output along the fault dividing blocks of different age.

## CONCLUSIONS

A total of 18 new measurements were made within the south part of the Gulf of Mexico, and 13 were made in the west part of the Caribbean Sea. Estimated heat flow values for the Gulf of Mexico (Campeche transect) are in the range of 37–66 mW/m$^2$ and for the Caribbean Sea (Yucatan transect) are in the range 24–139 mW/m$^2$. From numerical modeling, we obtained averages for the "deep" heat flow of 51 mW/m$^2$ for the Campeche transect and 38 and 69 mW/m$^2$ for two different basins in the Yucatan transect.

Observed variations of heat flow are caused by the influence of the bottom topography and by the contrasting thermal conductivities of different elements within the geological section. The bottom topography is a predominant disturbing factor in the Campeche transect.

"Deep" heat flow values within the Yucatan transect reflect the difference in type and age of Earth's crust. These heterogeneities must be due to changes in the depth of thermal sources in the transition zone from continental crust of the Yucatan plate to oceanic basin. Only an abrupt positive anomalous heat flow value was observed in the middle part of the continental slope of the Yucatan peninsula. Our lack of sufficient spatial coverage here does not permit us to describe in detail the hydrothermal conditions prevailing in this area.

*Acknowledgments.* We acknowledge O. V. Avgustynyak, Yu. V. Shmelev, M. A. Perez and E. Lugo for their help in carrying out the measurements, the crew on board R/V *Akademik Nikolaj Strakhov*, D. A. Zlochevsky for taking part in numerical modeling of the data, N. A. Pal'shin for kindly providing us with a copy of his algorithm, and to M. Hernandez for typing numerous versions of the manuscript. This work would not have been possible without the cooperation of the Mexican Government. These include the Secretaria de Relaciones Exteriores, Port authorities in Veracruz, Ver. and Cozumel, Q. R., and related administration. Funding for the participation of Mexican scientist was provided partially by CONACYT and CICESE. We also thank two anonymous reviewers for their comments that substantially improved the content.

## REFERENCES

Alexandrov, A. L., Probe for measuring of geothermal gradient on the oceanic bottom (in Russian), *Izv. Akad. Nauk SSSR, Ser. Fiz. Zemli*, *12*, 72–76, 1972.

Antoine, J. W., and T. E. Pyle, Crustal studies in the Gulf of Mexico, *Tectonophysics*, *10*, 477–494, 1970.

Bertagne, S. A., Seismic stratigraphy of Veracruz Tongue, deep southwestern Gulf of Mexico, *Am. Assoc. Pet. Geol. Bull.*, *68*, 1894–1907, 1984.

Bhattacharyya, G. K., and R. A. Johnson, *Statistical Concepts and Methods*, John Wiley, New York, 1977.

Case, Y. E., and T. L. Holcombe, Geologic tectonic map of the Caribbean region, scale 1:2,500,000, NOAA, Boulder, Colo., 1980.

Courtney, R. C., and R. S. White, Anomalous heat flow and geoid across the Cape Verde Rise: Evidence for dynamic support from a thermal plume in the mantle, *Geophys. J. R. Astron. Soc.*, *87*, 815–867, 1986.

Deep Sea Drilling Project, Leg 10, *Initial Rep. Deep Sea Drill. Proj.*, *10*, 1973.

De Moustier, C., State of the art in swath bathymetry survey systems, in *Current Practices and New Technology in Ocean*

*Engineering. OED 13*, edited by G. K. Wolfe and P. Y. Chang, pp. 29–38, American Society of Mechanical Engineers, 1988.

Detrick, R. S., R. P. Von Herzen, B. Parson, D. Sandwell, and M. Dougherty, Heat flow observations on the Bermuda Rise and thermal models of midplate swells, *J. Geophys. Res.*, *91*, 3701–3723, 1986.

Dillon, J. B., Structural profile of the northwestern Caribbean, *Earth Planet. Sci. Lett.*, *17*, 77–86, 1972.

Drummond, K. J., Plate tectonic map of the circum-Pacific region, Circum Pac. Counc. for Energy and Miner. Resour., Houston, Tex., 1981.

Edgar, N. T., J. I. Ewing, and J. Hennion, Seismic refraction and reflection in the Caribbean Sea, *Am. Assoc. Pet. Geol. Bull.*, *55*, 833–870, 1971.

Epp, D. E., P. J. Grim, and M. G. Langseth, Heat flow in the Caribbean and Gulf of Mexico, *J. Geophys. Res.*, *75*, 5655–5669, 1970.

Erickson, A. J., C. E. Helsley, and G. Simmons, Heat flow and continuous seismic profiles in the Cayman trough and Yucatan basin, *Geol. Soc. Am. Bull.*, *83*, 1241–1260, 1972.

Haenel, R., L. Rybach, and L. Stegena (Eds.) *Handbook of Terrestrial Heat-Flow Density Determination*, Kluwer Academic, Dordrecht, Netherlands, 1988.

Henry, S. G., and A. N. Pollack, Heat flow in the presence of topography: Numerical analysis of data ensembles, *Geophysics*, *50*, 1335–1342, 1985.

Hutchison, I., The effects of sedimentation and compaction on oceanic heat flow, *Geophys. J. R. Astron. Soc.*, *82*, 439–459, 1985.

Hyndman, R. D., E. E. Davis, and J. A. Wright, The measurements of marine geothermal heat flow by a multipenetration probe with digital acoustic telemetry and in-situ thermal conductivity, *Mar. Geophys. Res.*, *9*, 181–205, 1979.

Khain, V. E., *Regional Geotectonics* (in Russian), 548 pp., Nauka, Moscow, 1981.

Langseth, M. G., X. Le Pichon, and M. Ewing, Crustal structure of the mid-ocean ridges, 5, Heat flow through the Atlantic Ocean floor and convection currents, *J. Geophys. Res.*, *71*, 5321–5355, 1966.

Matveev, V. G., and A. A. Rot, New treatment of installation for automatization (BP) of marine geothermal researches on shelf, in *Geothermal Researches on Aquatorial Bottom* (in Russian), pp. 98–107, Nauka, Moscow, 1988.

Mossakovsky, A. A., G. E. Nekrasov, and S. D. Sokolv, Metamorphic Complexes and the problem of basement in alpine structures of the central sector of Cuba (in Russian), *Geotektonika*, *3*, 5–24, 1986.

Puscharovsky, Yu. M., On tectonics and geodynamics of the Caribbean region (in Russian), in *Tectonic Development of the Earth Crust and Lineaments*, pp. 124–132, Nauka, Moscow, 1979.

Rosencrantz, E., J. G. Sclater, and S. T. Boerner, Basement depths and heat flow in the Yucatan Basin and Cayman Trough, northwestern Caribbean: Implications for basin ages, in *CRC Handbook of Seafloor Heat Flow*, edited by J. A. Wright and K. E. Louden, pp. 257–261, CRC Press, Boca Raton, Fla., 1989.

Rot, A. A., and V. G. Matveev, Digital system for thermal conductivity measurements (in Russian), *Prib. Sist. Upr.*, *4*, 24–25, 1984.

Smith, L. A., and B. McNeely, Summary of leg 10, biostratigraphy, *Initial Rep. Deep Sea Drill. Proj.*, *10*, 731–736, 1973.

Von Herzen, R., and A. E. Maxwell, The measurements of thermal conductivity of deep-sea sediments by needle-probe method, *J. Geophys. Res.*, *64*, 557–1563, 1959.

Von Herzen, R., and S. Uyeda, Heat flow through the eastern Pacific Ocean floor, *J. Geophys. Res.*, *68*, 4219–4250, 1963.

Wadge, G., T. A. Jackson, M. C. Isaacs, and T. E. Smith, The ophiolithic Bath-Dundrobin Formation, Jamaica: Significance for Cretaceous plate margin evolution in the northwestern Caribbean, *J. Geol. Soc. London*, *139*, 321–333, 1982.

Wang, K., and A. E. Beck, Heat flow measurements in lacustrine or oceanic sediments without recording bottom temperature variations, *J. Geophys. Res.*, *92*, 12,837–12,845, 1987.

Worzel, J. L., R. Leydon, and M. Ewing, Newly discovered diapirs in the Gulf of Mexico, *Am. Assoc. Pet. Geol. Bull.*, *52*, 1194–1203, 1968.

R. Fernandez, Department of Applied Geophysics, CICESE, P.O. Box 4843, San Ysidro, CA 92073.

M. D. Khutorskoy, V. I. Kononov, and B. G. Polyak, Geological Institute of the Academy of Sciences of the USSR, Moscow, USSR.

V. G. Matveev and A. A. Rot, Polytechnical Institute, Kuybyshev, USSR.

(Received January 30, 1989;
revised July 20, 1989;
accepted June 27, 1989.)